Water Resources Research

RESEARCH ARTICLE
10.1029/2022WR033742

Layered Green and Ampt Infiltration With Redistribution

Peter La Follette[1,2], **Fred L. Ogden**[2], **and Ahmad Jan**[1,2]

[1]Lynker, Boulder, CO, USA, [2]Office of Water Prediction, National Oceanic and Atmospheric Administration, Tuscaloosa, AL, USA

Key Points:

- The Richards equation (RE) is widely used to simulate infiltration but often presents computational challenges
- We developed a Layered Green and Ampt with Redistribution (LGAR) approach that compares well against RE infiltration predictions
- The LGAR method is unconditionally stable with guaranteed mass conservation and is designed for semi-arid and arid areas

Supporting Information:

Supporting Information may be found in the online version of this article.

Correspondence to:

P. La Follette,
plafollette@lynker.com

Citation:

La Follette, P., Ogden, F. L., & Jan, A. (2023). Layered Green and Ampt infiltration with redistribution. *Water Resources Research*, *59*, e2022WR033742. https://doi.org/10.1029/2022WR033742

Received 26 SEP 2022
Accepted 31 MAR 2023

Author Contributions:

Conceptualization: Peter La Follette, Fred L. Ogden
Data curation: Peter La Follette, Fred L. Ogden, Ahmad Jan
Formal analysis: Peter La Follette, Fred L. Ogden
Investigation: Peter La Follette, Fred L. Ogden, Ahmad Jan
Methodology: Peter La Follette, Fred L. Ogden, Ahmad Jan
Project Administration: Fred L. Ogden
Resources: Peter La Follette, Fred L. Ogden

Abstract Numerical solution of the one-dimensional Richards equation (RE) accurately partitions precipitation into infiltration and runoff in capillary dominated soils. However, its application sometimes requires significant computational effort and presents reliability challenges. The Green and Ampt (G&A) approach represents a conservative and efficient method to calculate one-dimensional infiltration but is limited to deep, well drained, uniform, non-layered soils for a single rainfall event. The original G&A model and subsequent advancements represent wetting fronts as discrete objects, rather than discretizing the model domain in space, yielding a computationally simpler model than the RE. This paper describes an extension of the G&A method into layered soils on a continuous basis that we call Layered Green and Ampt with Redistribution (LGAR). Assumptions employed in the derivation include: uniform soil hydraulic properties within layers, single-valued capillary head at the interface between soil layers, and no influence of groundwater table on soil moisture. Wetting fronts advance due to the combined effects of gravity and wetting front capillary drive in a layered soil profile. Results of multi-month continuous LGAR simulations of infiltration using forcing and soil hydraulic data from USDA SCAN sites are compared against infiltration calculated using the HYDRUS-1D RE solver using standard metrics. The assumptions employed in deriving the LGAR method limit its application to situations where cumulative potential evapotranspiration is greater than cumulative precipitation, typical of arid or semi-arid conditions. LGAR is a mass-conservative, computationally efficient, reliable and reasonably accurate method for simulating infiltration over extended time periods compared to the numerical solution of the RE in layered soils in arid and semi-arid regions.

Plain Language Summary In arid and semi-arid regions the groundwater table is typically far below the land surface, and the process of infiltration divides rainfall into soil moisture and surface runoff. Previous extensions of the Green and Ampt (1911, https://doi.org/10.1017/s0021859600001441) infiltration method allow accurate calculation of infiltration into a layered soil for short time periods. This paper shows a novel extension that calculates infiltration in layered soils on a continuous basis using a Green and Ampt like method. This development represents an advance because it provides an accurate, mass-conserving, computationally efficient and reliable method to calculate infiltration in arid and semi-arid landscapes where stormflow generation is often dominated by layered soil properties.

1. Introduction

Green and Ampt (1911) applied physical reasoning backed by their knowledge of soil hydraulics to develop their method to predict vertical infiltration of water into a deep, well-drained, homogeneous soil with a uniform initial water content. Under these assumed conditions, particularly in finer textured soils, the G&A approach is remarkably accurate. Green and Ampt developed their method over 10 years before the first published instance of the Richards equation (RE). The RE was first published by Richardson (1922), and was separately published by Richards (1931); it is alternatively known as the Richardson-Richards equation, or RRE, as in Zha et al. (2019). See Raats and Knight (2018) for a discussion of the history and naming conventions of this equation. Although it has limitations (e.g., inability to describe macropore flow, hysteretic conductivity due to wetting-drying cycles, etc.), the RE is widely acknowledged as the most appropriate equation for simulating the infiltration process into capillary dominated, low Bond Number soils (Or, 2008).

The RE is a nonlinear partial differential equation that is usually applied to solve the temporal evolution of soil moisture at discrete points in space. Parameters used in the RE representing soil hydraulic properties potentially vary over 10 orders of magnitude. These are further used in empirical power (highly nonlinear) functions describing soil hydraulics. Because of this strong non-linearity, small changes in soil moisture can cause large changes

Software: Peter La Follette, Fred L. Ogden, Ahmad Jan
Supervision: Fred L. Ogden
Validation: Peter La Follette, Fred L. Ogden
Visualization: Peter La Follette, Fred L. Ogden, Ahmad Jan
Writing – original draft: Peter La Follette
Writing – review & editing: Peter La Follette, Fred L. Ogden, Ahmad Jan

in soil hydraulic properties, which renders RE solutions extremely sensitive to moisture content errors in certain circumstances.

Except in the simplest of cases, the RE requires numerical solution using a spatial discretization. Researchers seek to improve the stability, accuracy, and computational efficiency of these numerical solutions. Farthing and Ogden (2017) provide a summary of the current state of numerical RE solvers.

Many stability and reliability challenges arise in RE solvers in the case of infiltration into drier, fine-textured soils that cause sharp wetting fronts. The representative elementary volume (REV) for unsaturated soil hydraulic properties is on the order of 100–10,000 pore volumes (Sinai & Dirksen, 2006). The use of discretization larger than the REV can produce large errors in calculated soil hydraulic properties and reduced solution accuracy. Accurate RE solutions require domain discretization on the order of centimeters to accurately simulate wetting front dynamics (Downer & Ogden, 2004). All these factors render use of the RE implausible for simulating infiltration at thousands or millions of points using appropriate discretizations.

For this reason, the search for approximate methods that mimic the numerical solution of RE is a longtime area of research. The first extension to the G&A method involved extension of the method into layered soils. Early examples include Warrick and Yeh (1990). Selker et al. (1999) derived an analytical G&A solution for vertical 1-D infiltration into soil exhibiting linear, power law, or exponential reduction in permeability with depth after Beven (1982, 1984).

The first method to extend the G&A infiltration method to simulate multiple rainfall events was published by Smith et al. (1993) for a uniform soil. They extended the Smith and Parlange (1978) infiltration model, of which G&A is a special case, to simulate infiltration during multiple periods of rainfall with intervening periods of no or low intensity rainfall below the potential infiltration rate. The related approach developed by Corradini et al. (1994) was modified by Ogden and Saghafian (1997) to include explicit calculation of the capillary drive, specifically to modify the G&A capillary head term for unsaturated flow. They called their method Green and Ampt with Redistribution, or GAR. An extension of the GAR solution by Lai et al. (2015) improved the original method by coupling the vadose zone to a shallow water table. Coupling to groundwater was accomplished using a finite moisture content discretization (Talbot & Ogden, 2008) solution of the advection-like term of the Soil Moisture Velocity Equation (Ogden et al., 2017).

Since the introduction of the GAR model in 1997, many notable contributions to multilayer G&A - like modeling appeared in the literature. Corradini et al. (2000) presented a multilayer vadose zone model that partitioned precipitation into infiltration and runoff, albeit with a different algorithm for wetting front propagation than is used in LGAR. Chu and Mariño (2005), Liu et al. (2008), and Corradini, Morbidelli, et al. (2011) developed multilayer infiltration models that accounted for unsteady rainfall, where further advancements by Corradini, Flammini, et al. (2011) allowed for the stochastic representation of hydraulic conductivity in layered soils and therefore greater utility at the field scale. Ma et al. (2011) modeled the effects of entrapped air on G&A—like infiltration in a layered soil context. Mohammadzadeh-Habili and Heidarpour (2015) provided a model that simulates the infiltration rate of water into layered, unsaturated soil, assuming a fixed ponded depth of water on the soil surface. Mohammadzadeh-Habili and Heidarpour (2015) also provided a literature review on multilayer G&A—like models prior to their work, where the first six citations in this paragraph, among others, were included in their review. Deng and Zhu (2016) demonstrated how parameters from multiple soil layers can be upscaled, allowing for an effective multilayer representation of infiltration in a layered soil scenario with one representative set of soil parameters. Cui and Zhu (2017) presented a model for multilayer infiltration in sloping soils, where an empirical relationship between saturated and effective hydraulic conductivities improved infiltration simulations. Chen et al. (2019) developed a G&A - like infiltration model that further allowed for the representation of an unsaturated wetting front in scenarios where fine soil is above coarse soil, via two empirical parameters.

To the best of our knowledge, none of the published multilayer extensions to the Green and Ampt method encompass all of the features considered in this development of a generalized continuous infiltration model for multi-layered soils. With the LGAR method, we aimed to generalize the GAR concept to function on an arbitrary number of soil layers for continuous simulation of infiltration in response to any number of rainfall events. The method described in this paper considers the influences of ponded head, actual evapotranspiration, and allows for both unsaturated and saturated wetting fronts. The method also allows simulation of any number of wetting fronts.

2. Objectives

Hydrologic modeling of landscapes where infiltration partitions precipitation into soil moisture and surface runoff requires accurate simulations of infiltration. Such landscapes most commonly appear in arid and semi-arid regions, tilled lands (Wheater & Evans, 2009), and urbanized areas (Bocskor et al., 2017). Operational flood forecasting models further require computational speed and reliability. One-dimensional modeling of vadose zone processes is often acceptable because lateral unsaturated flow does not travel significant distances during interstorm periods (Or et al., 2015).

Because of the ubiquity of layered soils, the use of infiltration methods valid only for uniform soils represents a structural error in hydrologic models. While numerous RE solvers exist, computational expense and solution reliability make these unsuitable for use in large-scale operational forecasting models. This paper reports on development of a parsimonious, conservative, stable, efficient G&A-like solution for continuous simulation of 1-D infiltration in soils with an arbitrary number of layers. Parsimony is assured by requiring no more soil parameters than the RE solution requires. Evaluation involved comparing the LGAR method against the well-known HYDRUS-1D Richards equation solver applied using the same soil parameters and forcings. Comparisons against observations, which will include further detail incorporated into the LGAR concept, remain topics for future research.

3. Methods

This section describes the theory behind and development of a layered Green and Ampt with redistribution method. It begins by presenting the RE, the complete description of vertical (1-D) infiltration into capillary dominated low Bond number (fine textured, non-macroporous soils). The Soil Moisture Velocity Equation form of the RE is used next to derive the Green and Ampt equation, clearly showing the portion of the RE is omitted in the G&A approach. This is followed by the derivation of the Layered Green and Ampt with Redistribution method.

3.1. Fundamental Theory and Derivation of the Green and Ampt Model From the RE

The 1-D mixed (water content θ and capillary head ψ) form of the RE is:

$$\frac{\partial \theta}{\partial t} = \frac{\partial}{\partial z}\left[K(\theta)\left(\frac{\partial \psi(\theta)}{\partial z} - 1\right)\right] \tag{1}$$

where z is the vertical coordinate (positive downward) [L], t is time [T], θ is the volumetric soil moisture content [−], $\psi(\theta)$ is the empirical soil capillary head constitutive relationship [L], and $K(\theta)$ is the empirical unsaturated hydraulic conductivity constitutive relationship [L T^{-1}].

Starting with Equation 1, Ogden et al. (2017) derived what they called the "Soil Moisture Velocity Equation" (SMVE) through a change in dependent variable from θ to the depth of a particular moisture content Z_R using the cyclic chain rule. The SMVE is a kinematic equation describing the speed at which a particular moisture content θ advances into an unsaturated soil. Defining this speed as change in position of a moisture content point on a wetting front Z_R with time t is, the SMVE is:

$$\left.\frac{\partial Z_R}{\partial t}\right|_\theta = \frac{\partial K(\theta)}{\partial \theta}\left[1 - \frac{\partial \psi(\theta)}{\partial z}\right] - D(\theta)\frac{\frac{\partial^2 \psi}{\partial z^2}}{\frac{\partial \psi}{\partial z}} \tag{2}$$

where $D(\theta) = K(\theta)\frac{\partial \psi}{\partial \theta}$ [L^2 T^{-1}] is the soil water diffusivity.

Equation 2 contains two terms on the right hand side. The first term describes the effects of gravity and the integrated (scalar) capillary drive associated with the change in water content across the wetting front on soil moisture advection. For this reason, the first term is called the "advection-like" term. The second term describes the soil moisture advection due to diffusion. Note the similarity between the second term and Fick's law of diffusion; this second term is called the "diffusion-like" term. In this term, the numerator describes the curvature of the wetting front capillary head profile, while the denominator represents the slope of the wetting front capillary profile. Note that in the case of a sharp wetting front, the denominator of the second term $\frac{\partial \psi}{\partial z} \to \infty$, making the "diffusion-like" term vanish, and the movement of soil moisture becomes solely a function of the first term.

The method of lines replaces partial derivatives with finite-differences:

$$\left.\frac{dZ}{dt}\right|_{\theta_s} = -\frac{K(\theta_s) - K(\theta_i)}{\theta_s - \theta_i}\left[\frac{-\psi_{wf}}{Z} - 1\right] \tag{3}$$

where ψ_{wf} is the integrated capillary drive between θ_s and θ_i of a sharp, saturated wetting front located at a depth Z in the soil.

Assuming a small value of θ_i such that $K(\theta_i)$ is negligible, $\Delta\theta = (\theta_s - \theta_i)$, defining the G&A capillary head parameter as H_c, defining the cumulative infiltration $F = Z\Delta\theta$, and defining the potential infiltration rate f_p (so that $f_p = \frac{dF}{dt}$) under continuously wet surface conditions as $\frac{dZ}{dt}\Delta\theta$, the result is the Green and Ampt (1911) equation:

$$f_p = K_s\left(\frac{H_c\Delta\theta}{F} + 1\right) \tag{4}$$

We can calculate the rate at which the wetting front advances, $\frac{dZ}{dt}$:

$$\frac{dZ}{dt} = \frac{K_s}{\Delta\theta}\left(\frac{H_c}{Z} + 1\right) \tag{5}$$

Visually, this appears as a saturated "piston" advancing downwards, as shown in the left panel of Figure 1.

Finally, note that the G&A infiltration model and subsequent models based on the G&A concept are designed for infiltration under isothermal conditions of solute-free pure water neglecting the flow of the gas phase. Therefore the effects of solutes, temperature, and flowing gases are not considered when simulating infiltration using G&A and similar approaches.

3.2. Layered Green and Ampt With Redistribution (LGAR)

The original G&A model represents its wetting front with a discrete depth - moisture pair, visualized as a rectangle. This model was later generalized to the Green and Ampt with Redistribution model, or GAR (Lai et al., 2015; Ogden & Saghafian, 1997). The GAR model retained that property of wetting front representation, but further allowed for the representation of multiple and unsaturated wetting fronts, extending the utility of the model. LGAR is an extension of the GAR concept to multilayer soil hydraulic scenarios. See Figure 1 for a visualization of wetting fronts in the original G&A model, GAR, and LGAR.

In the LGAR concept, a wetting front can be further defined as a region of sudden discontinuity in water content within a soil layer with respect to depth, where wetting fronts only advance downward. The LGAR model includes the features of GAR, namely that multiple and unsaturated wetting fronts are allowed, and extends the concept by allowing wetting fronts to advance across boundaries between soil layers. Multilayer wetting front advance is achieved by enforcing the condition where soil moisture directly above and below a layer interface must have the same capillary head value ψ. Another notable difference between LGAR and GAR is that GAR calculates both $\frac{d\theta}{dt}$ and $\frac{dZ}{dt}$ for each wetting front, whereas LGAR computes $\frac{dZ}{dt}$ and then updates the

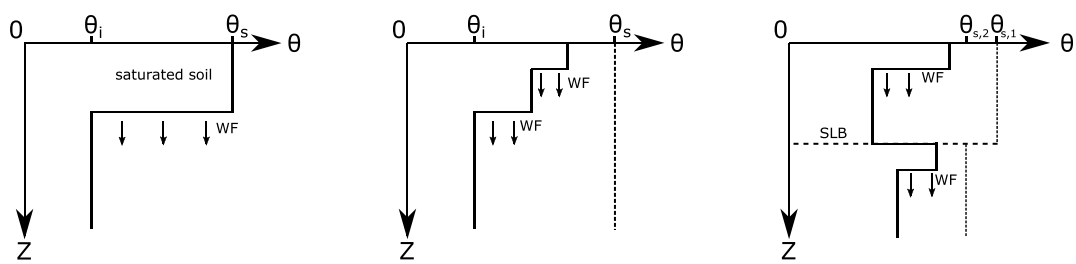

Figure 1. Visual schematics for the Green and Ampt infiltration model (left), the GAR model (center), and the LGAR model (right). "WF" indicates a wetting front and "SLB" indicates a soil layer boundary. Note that the G&A model allows for a single, saturated wetting front, the GAR model allows for multiple, unsaturated or saturated wetting fronts, and the LGAR allows for multiple saturated or unsaturated wetting fronts in a multilayer soil hydraulic scenario. Adjacent soil layers can have different hydraulic properties, for example, different saturated volumetric water contents, as shown in the right panel.

Table 1
Parameters Used by LGAR for Each Distinct Soil Layer

Parameter	Units	Description
θ_r	–	Residual volumetric water content
θ_s	–	Saturated volumetric water content
K_s	cm h^{-1}	Saturated hydraulic conductivity
α	cm^{-1}	van Genuchten parameter related to inverse of air entry pressure
n	–	van Genuchten parameter related to pore size distribution
m	–	van Genuchten parameter related to pore size distribution
L	cm	Soil layer thickness

Note. The use of these parameters allows for direct comparison of LGAR model outputs to those of HYDRUS-1D. It is required that $\alpha > 0$ and $n > 1$. Note that $m = 1 - n^{-1}$.

wetting front moisture via mass conservation. This section describes the various computational elements that allow LGAR to simulate soil moisture and partition precipitation. Section 3.3 shows examples of the LGAR method.

3.2.1. Soil Hydraulic Functions

The LGAR concept can use any monotonic soil moisture retention relation and associated hydraulic conductivity function. Model parameters necessary for each soil layer (see Table 1) and soil hydraulic functions are described in this subsection.

The integrated capillary suction across the wetting front, or capillary drive, G [L], from Morel-Seytoux and Khanji (1974), is given by:

$$G(\theta_b, \theta) = \frac{1}{K_s} \int_{\psi(\theta_b)}^{\psi(\theta)} K(\psi) d\psi \tag{6}$$

where θ [−] represents the volumetric water content of a wetting front, and θ_b represents the volumetric water content of the soil directly below the wetting front. Respectively, these θ values have corresponding capillary heads ψ and ψ_b. Volumetric water content θ as a function of capillary head ψ [L] is given by the following equation (Van Genuchten, 1980):

$$\theta(\psi) = \theta_r + \frac{\theta_s - \theta_r}{(1 + |\alpha\psi|^n)^m} \tag{7}$$

Note that negative values of ψ physically indicate unsaturated soil, and the above equation is valid for $\psi \leq 0$.

The hydraulic conductivity K [L T^{-1}] as a function of θ [−] is given by the following equation (Mualem, 1976; Van Genuchten, 1980):

$$K(\Theta) = K_s \Theta^l \left(1 - \left(1 - \Theta^{\frac{1}{m}}\right)^m\right)^2 \tag{8}$$

where the exponent l, an empirical pore-connectivity parameter, typically has a value of $\frac{1}{2}$ (Schaap & Van Genuchten, 2006). Relative water content Θ [−] is (Mualem, 1976):

$$\Theta = \frac{\theta - \theta_r}{\theta_s - \theta_r} \tag{9}$$

3.2.2. Wetting Front Initialization

At the beginning of an LGAR simulation, there is a single capillary head value throughout the entire vadose zone. When rainfall starts after a non-rainy period, a new wetting front is created in the topmost soil layer. Its initial depth is calculated as the "dry depth" h_{dry} [L], after Lai et al. (2015) using:

$$h_{dry} = 0.5(\tau + \sqrt{\tau^2 + 4\tau G(\theta_b, \theta_s)}); \qquad \tau = \frac{\Delta t K_s}{\theta_s - \theta_b} \tag{10}$$

where θ_b [−] in this case is the volumetric water content at the soil surface prior to precipitation, which is now the volumetric water content directly below the new wetting front. The time step size is given by Δt [T]. The maximum value for the dry depth is equal to the thickness of the topmost soil layer. The θ value of the newly created wetting front is calculated to conserve mass for the amount of water that infiltrated during its creation, taken as the precipitation intensity for the time step times the time step, unless this value yields a θ value greater than θ_s. In that case the θ value becomes θ_s and the water that does not infiltrate is retained on the surface.

3.2.3. Wetting Front Advance: Updating the State Variables Z and θ

After a wetting front is created, it advances downward in two steps. First, its $\frac{dZ}{dt}$ value, and accordingly new Z value, are calculated. Second, its θ value is updated, considering that the total amount of water relevant for each wetting front's advance can be expressed via mass conservation.

The first step is calculation of the speed of wetting front advance, $\frac{dZ}{dt}$. For a wetting front advancing in layer N, where layer number begins with 1 and increases with depth, this is given by:

$$\frac{dZ}{dt} = \frac{1}{\theta - \theta_b}\left(\frac{K_{s,N} G_N(\theta_b, \theta)}{Z} + K_c(\psi)\right) \tag{11}$$

where composite multilayer hydraulic conductivity K_c is given by:

$$K_c(\psi) = \frac{Z}{\sum_{n=1}^{N} \frac{T_n}{K_n(\theta_n(\psi))}} \tag{12}$$

and θ [−] is the volumetric water content of the wetting front, θ_b is the volumetric water content directly below the wetting front, $K_{s,N}$ [L T^{-1}] is the saturated hydraulic conductivity in the Nth layer, $K_n(\theta_n(\psi))$ is the hydraulic conductivity in layer n due to the soil moisture which has the same ψ value as the wetting front, that is, θ_n in layer n has the same capillary head as θ in layer N, T_n [L] is the thickness of soil in layer n which contains water that contributes to the expansion of the wetting front, Z [L] is the absolute depth of the wetting front, and the functions G and K have subscripts to indicate that their parameter values can differ between layers. While K_c is a multilayer composite hydraulic conductivity that will generally influence the propagation of a wetting front based on the soil characteristics in layers above the wetting front, we assume that capillary suction's effect on wetting front propagation is dominated by the soil hydraulics near the wetting front itself. Therefore, multilayer composite values are not used in the first term of Equation 11. Note that if a wetting front has spanned multiple layers, for all above the one in which the wetting front is currently, $T_n = L_n$, where L_n [L] is the thickness of soil layer n. This is because the wetting front has passed through the lower boundary of that soil layer. In the layer N which contains the wetting front, $T_n = T_N = Z - \sum_1^{N-1} L_n$.

After calculation of $\frac{dZ}{dt}$, we update the wetting front depth. Note that Equation 11 is valid for wetting fronts that advance within the top layer as well as wetting fronts advancing in deeper layers. In the event that this equation is used to calculate wetting front advance within the top layer, this equation reduces to the equation for $\frac{dZ}{dt}$ for a wetting front in GAR (Ogden & Saghafian, 1997).

After updating Z, we calculate a new θ value for the wetting front by imposing two conditions. First, conservation of mass accounting for the wetting front's advance, and second, requiring equal capillary head in the soil moisture directly above and below any layer interfaces crossed by the wetting front.

First, the total mass of water relevant for the advance of the wetting front M [L], at time step i, is:

$$M_i = \sum_{n=1}^{N} (\theta_n(\psi_i) - \theta_n(\psi_{b,i}))T_n \tag{13}$$

Here, the i subscript indicates the values of variables at the ith time step, the wetting front is in layer N, ψ is the capillary head of the wetting front, and ψ_b is the capillary head directly below the wetting front. Note that $\theta_n(\psi)$ yields the soil moisture in layer n corresponding to ψ, such that θ is a function of ψ.

For the wetting fronts that are deeper than the most superficial one, conservation of mass for soil moisture relevant for wetting front advance requires:

$$M_i = M_{i+1} \tag{14}$$

Given that M_i is already known, and given that Z_{i+1} is already known from solving for $\frac{dZ}{dt}$, the new psi value ψ_{i+1} can be iteratively solved with Equations 13 and 14. This yields the new θ value for the wetting front.

Equation 14 can be used for all wetting fronts, except for the wetting front nearest to the soil surface. In the LGAR concept, both evapotranspiration and surface infiltration fluxes affect the mass balance for this wetting front. Therefore, the conservation of mass for the top most wetting front instead requires:

$$M_i + (r - AET)\Delta t = M_{i+1} \tag{15}$$

where r [L T^{-1}] is the infiltration rate (which is either equal to or less than the infiltration capacity; see Equation 16) and AET [L T^{-1}] is the rate of actual evapotranspiration. Once AET and infiltration are calculated, this equation can be used in the same way as Equation 14 to update the volumetric water content of the top most advancing wetting front.

3.2.4. Calculation of Infiltration

LGAR uses the same concept of infiltration capacity as in the original G&A model and as in GAR. Specifically, if precipitation is less than the infiltration capacity, then all of the precipitation infiltrates and becomes soil moisture. In the event that precipitation is greater than the infiltration capacity, then water accumulates on the soil surface at a rate equal to the precipitation intensity minus the infiltration capacity, and water infiltrates into the soil at a rate equal to the infiltration capacity. The infiltration capacity in LGAR is controlled by the top most wetting front. The infiltration capacity f_p [L T^{-1}] is given by:

$$f_p = \frac{K_{s,N} G_N(\theta_b, \theta_{s,N})}{Z} + \frac{Z}{\sum_{n=1}^{N} \frac{T_n}{K_{s,n}}} \tag{16}$$

where Z [L] is the depth of the top most wetting front, θ_b [−] is the volumetric water content directly below this wetting front, and $K_{s,N}$ [L T^{-1}] is the saturated hydraulic conductivity of layer N, where the wetting front is advancing in layer N, and T_n is the thickness of soil layer n that contains water used for the expansion of the wetting front (also see Equation 11). Note that in the case of a wetting front in the topmost soil layer, Equation 16 becomes the same equation as is used to calculate f_p in the GAR model (Lai et al., 2015; Ogden & Saghafian, 1997). When greater than 0, infiltration increases the amount of water relevant for the mass balance of the top most wetting front via Equation 15.

3.2.5. Calculation of AET From PET

While the simulation of infiltration and soil moisture profiles technically does not inherently require incorporation of evapotranspiration, LGAR was designed for arid and semi-arid areas, in which fluxes from the vadose zone are typically dominated by actual evapotranspiration (AET). Therefore, LGAR requires precipitation and potential evapotranspiration (PET) data to run, with AET calculated from PET using a method that accounts for the limiting effect of soil moisture. Because we compared the LGAR model against HYDRUS-1D, we applied the same S-shaped function used in HYDRUS-1D (Simunek & Sejna, 2018):

$$AET = PET \frac{1}{1 + (\psi/\psi_{50})^3} \tag{17}$$

Here, ψ [L] is the capillary head at the soil surface and ψ_{50} [L] is the capillary head at which $AET = 0.5\ PET$. In LGAR, the AET demand is taken only from the wetting front with a ψ value closest to 0, which is also necessarily the top most wetting front. AET demand is extracted by reducing the moisture content of this wetting front. If this wetting front spans multiple layers, moisture is extracted in such a way that the ψ value on either side of a

soil layer boundary is the same after extraction. In both LGAR and HYDRUS-1D, we calculated ψ_{50} to be the capillary head corresponding to the volumetric water content for the top layer which is halfway between the wilting point, which we assume has a capillary head of −15 atm, and field capacity. We assume field capacity has a relative water content of 0.75, while other values are possible, depending on soil type. Note that the exponent in the denominator has a value of 3, which is the recommended value according to HYDRUS-1D (Simunek et al., 2005).

While we choose this PET correction method in order to approximate PET as simulated by HYDRUS, there are notable differences between how ET is handled in LGAR and HYDRUS-1D. HYDRUS-1D has the option to partition PET into potential evaporation and potential transpiration, which are separately corrected to actual evaporation and actual transpiration. HYDRUS-1D uses Equation 17 to calculate actual transpiration, and further uses the concept of relative rooting density, which is specified per node, on a scale from 0 to 1. Therefore in HYDRUS-1D, Equation 17 is applied for each node with roots. HYDRUS-1D also has a separate equation which calculates bare soil evaporation. In contrast, LGAR combines evaporation and transpiration, much like many other hydrologic models. LGAR does not explicitly represent a root zone as is possible in HYDRUS-1D, and instead leverages the assumption that evapotranspiration demand in unsaturated soils is preferentially drawn from soils that have a capillary head closer to 0. In the context of LGAR, this will always be the top most wetting front. Finally, please note that in HYDRUS-1D, the parameter ψ_{50} is written h_{50}, which we changed for consistency with the LGAR model.

3.2.6. Wetting Front Merging

In Equation 11, the speed of wetting fronts with a higher θ value is usually faster than those with smaller θ values. This causes wetter, more superficial wetting fronts to overtake deeper, drier wetting fronts. In this event, the overtaking wetting front merges with the overtaken front when they reach the same depth. Merging also occurs when the *AET* taken from the top most wetting front reduces the volumetric water content of that wetting front to equal the volumetric water content directly below in the same layer. In this case, the wetting fronts merge in a mass conservative way.

3.2.7. Wetting Fronts That Cross Layer Interfaces and the Lower Boundary

During a time step when the calculated $\frac{dZ}{dt}$ of a wetting front causes it to advance into another soil layer, the water that propagated into the layer below is assumed to create a new wetting front in that layer. The wetting front is no longer in the more superficial of the two layers. The method requires the new wetting front to have the same capillary head as the soil moisture profile directly above it.

When a wetting front advances to the bottom of the model domain, the amount of water that surpassed the model lower boundary for a given time step is considered lost through the model lower boundary. However, correct implementation of actual evapotranspiration prevents this from happening in arid and semi-arid climates, except under unusually wet conditions. When this does happen, the value for $\frac{dZ}{dt}$ for the wetting front that exceeds the lower boundary is usually small. Although LGAR was initially developed with a unit head gradient (free drainage) lower boundary condition, LGAR is intended for use in arid or semi-arid environments in the absence of a near-surface water table. In those environments, recharge to groundwater can often be neglected. When appropriately applied under the conditions assumed in the LGAR derivation, the effect of lower boundary condition on surface partitioning of precipitation is not significant. In cases where groundwater interactions such as those due to a rising near-surface water table or thin soil over relatively impervious bedrock, the LGAR method is not appropriate. In short, conceptually, our lower boundary condition is no-flow, but technically some small amount water can leave the vadose zone through the lower boundary as a model artifact.

3.2.8. Ponded Head

The development presented up to now did not consider the effect of ponded water on the land surface on infiltration capacity or wetting front advance. The effect of ponded head h_p [L] is to increase the capillary drive G of the top-most wetting front by an amount equal to h_p.

This yields the general equations for the advance of wetting fronts which are affected by ponded head, which are similar to Equations 11 and 16:

$$\frac{dZ}{dt} = \frac{1}{\theta - \theta_b}\left(\frac{K_{s,N}(h_p + G_N(\theta_b, \theta))}{Z} + \frac{Z}{\sum_{n=1}^{N} \frac{T_n}{K_n(\theta_n(\psi))}}\right) \tag{18}$$

$$f_p = \frac{K_{s,N}(h_p + G_N(\theta_b, \theta_{s,N}))}{Z} + \frac{Z}{\sum_{n=1}^{N} \frac{T_n}{K_{s,n}}} \quad (19)$$

In all the following experiments, $h_p = 0$, so any rainfall not infiltrating is removed each time step and accounted for as surface runoff.

3.2.9. Assumptions Necessary for LGAR Development

As described in Section 3.2.7, the lower boundary condition for LGAR is effectively no-flow. That is, LGAR is developed for use in areas where recharge to groundwater will be negligible, where groundwater itself will essentially have no impact on wetting front propagation and therefore on infiltration partitioning. This realistically occurs in arid or semi-arid areas, where groundwater is potentially hundreds of meters deep. These areas are also characterized by the property of cumulative PET being substantially greater than cumulative precipitation. In the event that cumulative PET is less than cumulative precipitation, it easily could be the case that vadose zone dynamics would be impacted by the presence of a shallow water table, necessitating a more complex lower boundary condition (Lai et al., 2015). Development of such a condition is planned for future work. Finally, if LGAR is currently used in environments where cumulative PET is less than cumulative precipitation, by definition the vadose zone will eventually become saturated, given the no-flow lower boundary condition.

Note also that LGAR is generally unable to represent regions of larger capillary head below regions of smaller capillary head, for example, wetter regions under drier regions in the same soil layer. This is due to the fact that a wetting front always advances downward, always begins as wetter than the one directly below it, and merges with the wetting front below once it reaches a sufficient depth. This precludes certain hydraulic scenarios, for example, the existence of a perched water table forming at the interface of a deeper, less permeable layer, which does not extend to the soil surface. The LGAR method can however produce a perched water forming at a layer interface that does extend to the soil surface. Future work will allow for the representation of drier over wetter regions of soil moisture in the same layer.

3.3. Examples Showing the LGAR Method

This section provides an example simulation of LGAR and shows detailed example calculations of advance and redistribution based on mass balance. While the following explanation relies on figures, the we encourage the reader to watch animations of the LGAR method at: https://www.hydroshare.org/resource/46747d77d0ce4995b1e1d58384e15a09/.

Figure 2 shows the soil moisture profile and model fluxes as simulated by the LGAR method, given forcing data consisting of two precipitation pulses and zero PET. The soils fine downward, such that K_s decreases with depth, as is commonly observed (Beven, 1982, 1984). The precipitation intensity has in this case been selected to always be less than f_p, such that there is no runoff.

At the start of the simulation, in panel A, the capillary head is set to −100 cm everywhere in the domain, and there are no wetting fronts. Despite having the same capillary head everywhere, the three different soil layers, delineated with dashed lines, show different volumetric water contents. This is because these layers have distinct hydraulic parameters and therefore have differing θ values for the same ψ. Panel B shows conditions after the end of the first precipitation pulse, which remains within the top layer by time = 4.5 hr. This wetting front eventually propagates into the second layer, as shown in panel C. Note that the area of the purple polygon in the depth—moisture plot in panel C has the same area as the purple rectangle in the depth—moisture plot in panel B, representing mass conservation for this wetting front in the absence of precipitation and ET. Further note that all purple shaded soil moisture in panel C has the same ψ value, further showing the required condition that soil moisture directly above and below a layer interface must have the same capillary head.

In panel D, we see a new wetting front that is advancing within the topmost soil layer. Because this wetting front was created by a distinct precipitation event, it does not contribute to the purple shaded mass of water and instead it creates a new conservative mass shaded with a different color (orange). By time = 17 hr (panel E), this new wetting front has propagated to the second layer as well. By time = 50 hr (panel F), the wetter, orange wetting front has caught up to the drier, purple wetting front, and they merged in such a way that total mass was

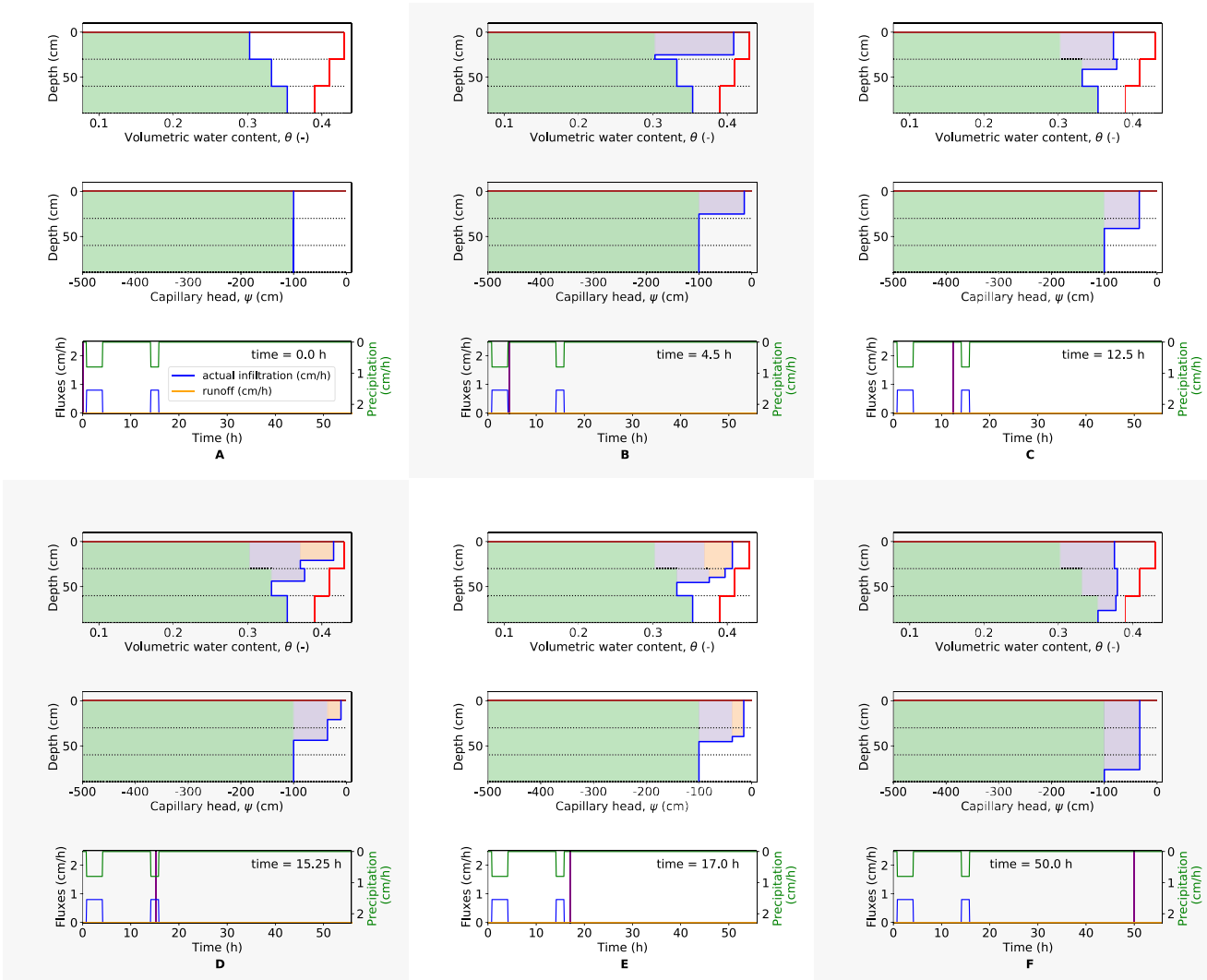

Figure 2. A series of six illustrations showing profiles of water content θ and capillary head ψ at six different times during infiltration into a three layered soil in response to two rainfall pulses. The solid blue line in these profiles represents soil moistures or capillary heads simulated at different time steps, and the horizontal dotted lines indicate layer boundaries. The red line represents the saturated water content for each layer. Note that, for each Z - θ profile, the color used denotes capillary head. Further, all soil moisture of a given color involves a single mass balance calculation. Soil moisture present at the start of the simulation is shown as green. Soil moisture due to one of the two discrete precipitation pulses is denoted using purple or orange. In the last frame, the wetting front previously identified as orange has merged with the purple-colored wetting front.

conserved. In other words, the sum of the areas of the orange and purple polygons in the depth—moisture plot in panel E is equal to the area of the purple polygon in the depth—moisture plot in panel F.

Next, we show the explicit computation of $\frac{dZ}{dt}$ for the two wetting fronts in Figure 2, panel E.

In Figure 3, there are two wetting fronts, both in the second soil layer, represented by purple and orange shaded water. Relevant variables for the advance of the shallower (orange shaded) wetting front are shown in the left panel, and relevant variables for the advance of the deeper (purple shaded) wetting front are shown in the right panel. Because both wetting fronts are in the second layer, they both use the same advance equation:

$$\frac{dZ}{dt} = \frac{1}{\theta - \theta_b}\left(\frac{K_{s,2}G_2(\theta_b,\theta)}{Z} + \frac{Z}{\frac{T_1}{K_1(\theta_1(\psi))} + \frac{T_2}{K_2(\theta_2(\psi))}}\right) \tag{20}$$

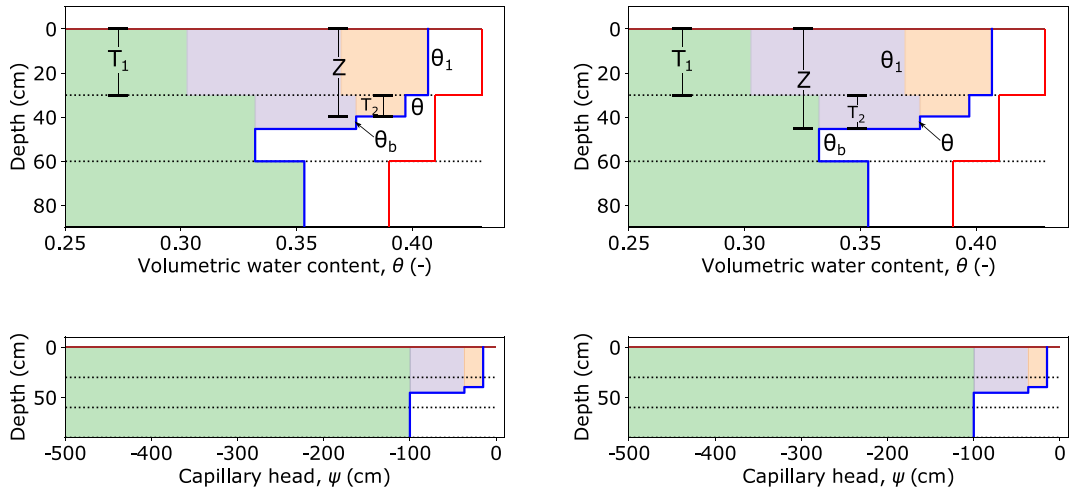

Figure 3. Visualization of variables relevant for the calculation of $\frac{dZ}{dt}$ for two wetting fronts. The left figures show variables for the higher wetting front and the right figures show variables for the lower wetting front, corresponding to panel E in Figure 2. Top panels show soil moisture profiles, and bottom panels show how the corresponding capillary head varies with respect to depth. The blue line represents LGAR simulated results, and the red line represents the θ_s value for each layer.

which is the application of Equation 11 when $N = 2$. However, the values used for θ, θ_b, θ_1, Z, and in this case T_2 differ depending on which wetting front's $\frac{dZ}{dt}$ value is being calculated. Because $N = 2$, $\theta_N = \theta_2 = \theta$.

Here we show an example calculation of the relevant mass of soil moisture for a wetting front's advance. This also corresponds to panel E in Figure 2.

In Figure 4, there are two wetting fronts, both in the second soil layer, represented by purple and orange shaded water. Relevant variables for the mass balance of the shallower (orange shaded) wetting front are shown in the left panel, and relevant variables for the mass balance of the deeper (purple shaded) wetting front are shown in the right panel. Because both wetting fronts are in the second layer, they both have the same general equation for M, from Equation 13, given in this case by:

$$M = (\theta_2(\psi) - \theta_2(\psi_b))T_2 + (\theta_1(\psi) - \theta_1(\psi_b))T_1 \tag{21}$$

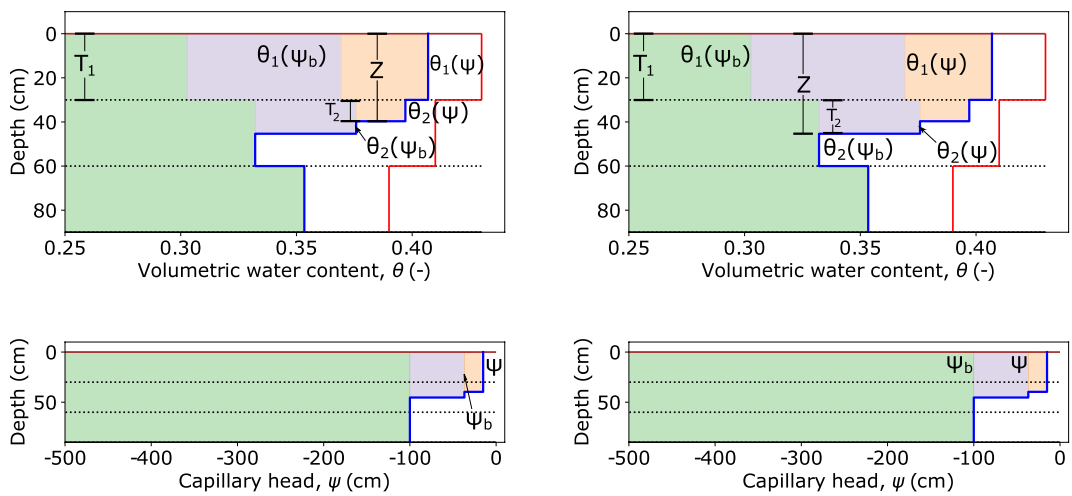

Figure 4. Visualization of mass balance calculation and relevant variables for two wetting fronts, corresponding to panel E in Figure 2. The blue line represents LGAR simulated results, and the red line represents the θ_s value for each layer. Top panels represent soil moisture profiles, and bottom panels show how the corresponding capillary head varies with respect to depth. Masses for components of wetting fronts can be visualized as rectangles in the moisture—depth plots.

Table 2
Parameters Used for Comparisons of LGAR and HYDRUS Using Idealized Data

Parameter	Layer	Test 1 value	Test 2 value	Test 3 value	Units
θ_r	1	0.078	0.034	0.057	–
	2	0.095	0.089	0.078	
	3	0.089	0.068	0.067	
θ_s	1	0.43	0.46	0.41	–
	2	0.41	0.43	0.43	
	3	0.43	0.38	0.45	
K_s	1	3.12	0.25	14.59	cm h^{-1}
	2	0.26	0.07	1.04	
	3	0.07	0.20	0.45	
α	1	0.036	0.016	0.124	cm^{-1}
	2	0.019	0.010	0.036	
	3	0.010	0.008	0.020	
n	1	1.56	1.37	2.28	–
	2	1.31	1.23	1.56	
	3	1.23	1.09	1.41	
L	1	10	10	10	cm
	2	30	30	30	
	3	30	30	30	

Note. Test 1, from layer 1 to 3, consisted of loam, clay loam, and silty clay loam; test 2 consisted of silt, silty clay loam, and silty clay; test 3 consisted of loamy sand, loam, and silt loam.

However, the values used for ψ, ψ_b, and T_2 differ depending on which wetting front's mass balance is being calculated. The total amount of water relevant for the mass balance for a wetting front advancing in the Nth layer can be represented by the total area of N rectangles in the depth—θ plot, where each layer contains one rectangle. Specifically, each term in Equation 15 represents the area of a rectangle, which has a width equal to $\theta_n(\psi) - \theta_n(\psi_b)$ and a height equal to T_n, where $T_n = L_n$ for layers above layer N and $T_n = T_N = Z - \sum_1^{N-1} L_n$ for layer N, the layer containing the wetting front.

Finally, updating the θ value for these wetting fronts requires the combinations of Equations 13 and 14. Note that in this case, the use of Equation 15 is not necessary because at this time there is zero precipitation and PET. This yields:

$$M_i = (\theta_2(\psi_{i+1}) - \theta_2(\psi_{b,i+1}))(Z_{i+1} - L_1) + (\theta_1(\psi_{i+1}) - \theta_1(\psi_{b,i+1}))L_1 \quad (22)$$

Since M_i is known, and Z_{i+1} is known from the calculation of $\frac{dZ}{dt}$, Equation 22 can be solved for ψ_{i+1}. Because both wetting fronts in Figure 4 are in the second layer, this equation is applicable to both, although again the specific variable values change. Because $\psi_{b,i+1}$ must also be known, wetting fronts are updated from deepest to shallowest.

4. Results

Comparison of the performance of the LGAR method and that of HYDRUS-1D involved simulations with idealized forcing data and simulations using observations of precipitation and soil properties. The simulations with idealized forcing data lasted 12 hr and served to demonstrate the functionality of LGAR in a detailed way. The simulations using measured precipitation data had durations of several months to demonstrate the practical applicability of the LGAR method. Multiple soil textures were tested in simulations using both idealized and observed precipitation forcings.

4.1. Simulations Using Idealized Forcing Data

Tests using idealized forcing datasets involved three different layered soil scenarios. In each case, there was a short precipitation pulse, starting 30 min into the simulation and lasting 25 min. This was followed by a longer precipitation pulse lasting 5 hr and 50 min, which started 4 hr and 55 min into the simulation. The precipitation intensity was the same for both pulses in each scenario and was selected such that the first, shorter pulse completely infiltrated into the soil while the second, longer pulse exceeded the potential infiltration rate during that pulse.

These tests were also designed such that the wetting front generated by the second precipitation pulse merges with the wetting front created by the first precipitation pulse. This allowed exploration of the ability of LGAR to approximate HYDRUS-1D where wetting front merging occurs in a layered soil system.

Table 2 shows the soil parameters for each scenario, Figure 5 shows cumulative infiltration and runoff from LGAR and HYDRUS-1D resulting from the three different scenarios, and Table 3 shows a variety of error statistics quantifying the accuracy of LGAR simulations. We assumed zero PET and the initial capillary head was set to −100 cm throughout the domain. Rain rates tested during scenarios 1, 2, and 3 were 2 cm hr^{-1}, 0.7 cm hr^{-1}, and 5 cm hr^{-1}.

4.2. Simulations Using Observed Precipitation Forcing

The LGAR method and HYDRUS-1D were also compared in three scenarios using observed precipitation data, and PET data calculated using the Priestly-Taylor method. These tests use soil hydraulic parameters and forcing

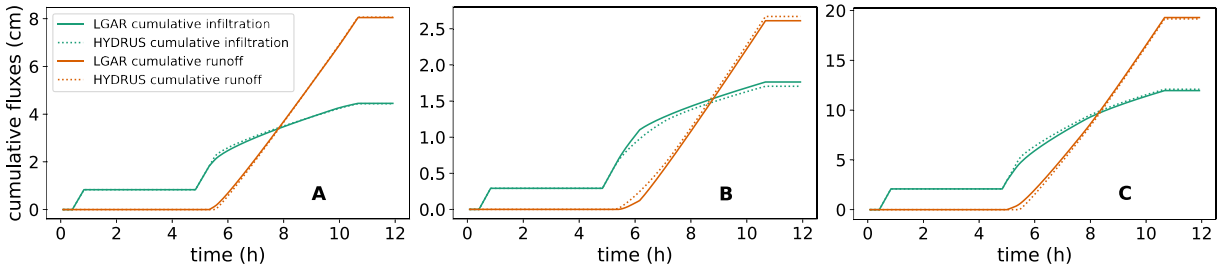

Figure 5. Cumulative infiltration as simulated by LGAR and HYDRUS-1D, where panel (a) shows test 1, panel (b) shows test 2, and panel (c) shows test 3.

data from USDA SCAN sites located in arid and semi-arid sites near Fort Assiniboine, MT, Phillipsburg, KS, and Bushland, TX. Soil hydraulic parameters for each simulation are listed in Table 4. In HYDRUS-1D, the root zone density linearly decreases with respect to depth, such that the top node has a relative rooting density of 1 and the bottom node has a relative rooting density of 0. Further, in HYDRUS-1D, PET was equally partitioned into potential evaporation and potential transpiration. The initial condition for each USDA SCAN simulation is uniform capillary head throughout the vadose zone, and this value is −300 cm for Fort Assiniboine and −2,000 cm for Phillipsburg and Bushland. Respectively, these sites had cumulative precipitation totals of 36.12, 99.09, and 25.98 cm for their simulation periods.

Figure 6 provides plots of the cumulative fluxes as simulated by the LGAR method and HYDRUS-1D. Results suggest a close match for runoff and infiltration. To further quantify the ability of LGAR to approximate the precipitation partitioning as simulated by HYDRUS-1D, Table 5 shows a variety of statistics comparing LGAR and HYDRUS-1D results.

5. Discussion

5.1. The LGAR Method Is Designed for Arid or Semi-Arid Areas

The LGAR method agreed quite well with HYDRUS-1D in terms of calculated infiltration, and to a slightly lesser extent runoff. Visually, it is apparent that both infiltration and runoff cumulative values match closely between the LGAR model and HYDRUS-1D at the USDA SCAN sites, as shown in Figure 6. Quantitatively, Table 5 shows that infiltration and runoff simulations from the LGAR model achieve good error statistics, typically achieving KGE and NSE values close to 1. Especially given that these are multi-month simulations, we interpret these results as evidence that LGAR partitions precipitation in a very similar way to HYDRUS-1D.

At the Fort Assiniboine site, the LGAR method compares quite favorably in terms of infiltration with NSE of 0.995 and KGE of 0.973. However, because runoff is the residual rainfall that does not infiltrate, and almost all the rainfall at this site is predicted by both HYDRUS-1D and LGAR to infiltrate, relatively small differences in infiltration can result in large differences in calculated runoff. At this site the difference in cumulative runoff was

Table 3
Error Metrics Describing the Differences Between LGAR and HYDRUS-1D Simulations for Short Simulations Using Idealized Precipitation Data

Test number	Flux	KGE (−)	NSE (−)	PBIAS (%)	RMSE (cm h^{-1})	LGAR cumulative (cm)	HYDRUS-1D cumulative (cm)	Difference (cm)
1	Infiltration	0.956	0.974	−0.33	0.092	4.45	4.44	−0.01
	Runoff	0.975	0.986	0.18	0.092	8.05	8.06	0.01
2	Infiltration	0.916	0.952	−3.47	0.044	1.76	1.70	−0.06
	Runoff	0.967	0.972	2.21	0.044	2.61	2.67	0.06
3	Infiltration	0.931	0.970	1.11	0.25	11.96	12.09	0.13
	Runoff	0.967	0.982	−0.70	0.25	19.29	19.16	−0.13

Note. Values in KGE, NSE, percent bias, and RMSE correspond to time series of infiltration and runoff, rather than time series of these variables cumulatively.

Table 4
Parameters Used for Comparisons of the LGAR Method and HYDRUS-1D Using Observed Forcing Data

Parameter	Layer	Fort Assiniboine	Phillipsburg	Bushland	Units
θ_r	1	0.0416	0.0648	0.0649	–
	2	0.0762	0.0831	0.0672	
	3	0.0574	0.0668	0.0823	
θ_s	1	0.4189	0.4513	0.4481	–
	2	0.4792	0.4773	0.4760	
	3	0.3986	0.4617	0.4782	
K_s	1	1.02	0.45	0.07	cm h^{-1}
	2	0.26	0.07	0.02	
	3	0.26	0.45	0.20	
α	1	0.02393	0.0031297	0.009567	cm^{-1}
	2	0.01648	0.0083272	0.005288	
	3	0.00458	0.0037454	0.004467	
n	1	1.3527	1.6858	1.379	–
	2	1.3086	1.299	1.5276	
	3	1.4243	1.6151	1.4585	
L	1	13	44	18	cm
	2	71	131	76	
	3	170	25	135	

Note. While three layers per site are used here, the LGAR method allows for any number of soil layers.

only 0.3 cm, but the NSE and KGE values were 0.821 and 0.688, respectively. Therefore, when precipitation is overwhelmingly partitioned into infiltration, small differences in infiltration values will still indicate a good objective function result, while these same magnitudes of difference can cause runoff results to achieve significantly lower accuracy metrics. Given that LGAR is designed for use in arid and semi-arid areas where the majority of precipitation will infiltrate, one can expect LGAR and HYDRUS simulations to typically yield better error statistics for infiltration as opposed to runoff.

The assumptions used to derive the LGAR method include a deep, well-drained soil without the presence of a near-surface groundwater table that requires use of the method in environments where percolation to groundwater is small. This is realistically achieved when potential evapotranspiration, on average, exceeds precipitation. In simulations using the LGAR method with $PET = 0$, the method was sensitive to choice of lower boundary condition. In tests using observed forcing data with $PET = 0$ and applying a free drainage lower boundary condition in both models, simulation results between the LGAR method and HYDRUS-1D diverged. This occurred because in a multilayer soil hydraulic scenario in the RE with no evapotranspiration, the capillary head toward the bottom of the model domain eventually became significantly larger than the capillary head at the top of the model domain. This increased the magnitude of free drainage as simulated by HYDRUS-1D, relative to the magnitude of free drainage as simulated by the LGAR method, ultimately leading to overall drier soils and therefore more infiltration simulated by HYDRUS-1D. In arid and semi-arid environments where percolation from to groundwater is almost always near zero, the choice of a no-flow lower BC is a realistic assumption. Future developments of LGAR will involve the development of a shallow groundwater module which interacts with the LGAR vadose zone domain, which will be useful for simulations in areas with more precipitation than potential evapotranspiration.

Figure 5 and Table 3 demonstrate that LGAR emulates RE precipitation partitioning results accurately for shorter simulations with negligible PET as well. While LGAR simulates shorter events accurately compared to HYDRUS-1D, when simulating longer events, PET must be included or else the vadose zone will eventually completely saturate.

5.2. Differences in ET Between the LGAR Model and HYDRUS-1D

While HYDRUS-1D and LGAR use similar schemes used to calculate PET from AET, they are not identical. HYDRUS-1D allows for separate representation of both potential evaporation and potential transpiration. Then, HYDRUS-1D separately corrects these to their actual values, respectively, using a bare soil evaporation routine

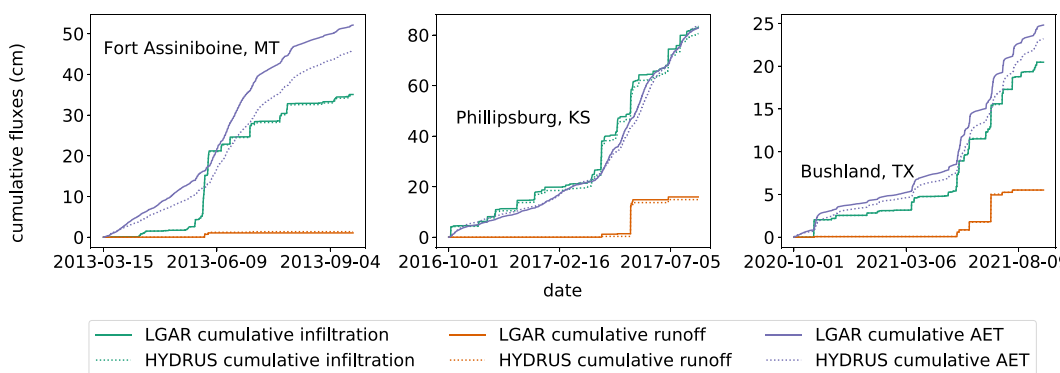

Figure 6. Cumulative fluxes as simulated by LGAR and HYDRUS, using observed forcing data.

Table 5
Error Metrics Describing the Differences Between LGAR and HYDRUS-1D Simulations

Location	Flux	KGE (−)	NSE (−)	PBIAS (%)	RMSE (cm h^{-1})	LGAR cumulative (cm)	HYDRUS-1D cumulative (cm)	Difference (cm)
Fort Assiniboine	Infiltration	0.973	0.995	−0.91	3.56E−3	35.06	34.75	−0.318
	Runoff	0.688	0.821	22.60	3.44E−3	1.055	1.363	0.308
Phillipsburg	Infiltration	0.954	0.979	−3.20	1.55E−2	83.153	80.577	−2.576
	Runoff	0.915	0.986	−7.07	1.53E−2	15.93	14.88	−1.05
Bushland	Infiltration	0.954	0.971	3.16E−2	4.95E−3	20.467	20.473	6.47E−3
	Runoff	0.985	0.969	−0.143	4.92E−3	5.518	5.510	−7.87E−3

Note. Values in KGE, NSE, percent bias, and RMSE correspond to time series of infiltration and runoff, rather than time series of these variables cumulatively.

and an S-curve method. Further, the specification of a rooting zone and relative root density per node allows for spatially detailed transpiration schemes. In contrast, LGAR uses only the S-curve method to simulate actual evapotranspiration, using the capillary head of the topmost wetting front. While such a method is relatively common among hydrologic models in general (i.e., simply computing AET is more common than partitioning AET into actual transpiration and actual evaporation), this difference from HYDRUS does evidently make the AET comparison the poorest of the simulated fluxes (see Figure 6). In some cases, for example, the Phillipsburg case, the difference in cumulative AET between the two models is small, and LGAR results even switch from under-to overestimation relative to the HYDRUS-1D result. However, when the initial capillary head is significantly closer to 0, for example, in the case of Fort Assiniboine, apparently the AET method used by LGAR predicts significantly more cumulative AET than the HYDRUS-1D method does. This suggests that the effect of bare soil evaporation is likely less significant than the effect of transpiration for wetter soils. Whatever the case, it will be the case that different ET regimes will be preferred in different climates: semi-arid climates will likely have a higher proportion of PET partitioned into potential transpiration than potential evaporation, when compared against arid environments. With the introduction of LGAR, we merely indicate that AET is an important flux to include; the optimization of ET schemes based on environment is an interesting topic for future research.

It is also interesting to note that the LGAR method and the HYDRUS-1D RE solver can well agree in terms of precipitation partitioning results while comparing poorly in terms of AET simulations, as the Fort Assiniboine simulations of Figure 6 shows. This is essentially due to the chosen rooting zone in HYDRUS. In the HYDRUS-1D simulations using USDA SCAN data, the relative rooting density per node decreases linearly with respect to depth, such that this value is 1 for the top node and 0 for the bottom node. Therefore the relative rooting density is lower for the deeper portions of the model domain, such that relatively little of the AET demand comes from these deeper soils in HYDRUS-1D. In contrast, LGAR removes water from the top most wetting front, which actually often spans all three layers—this scenario becomes more common when precipitation events and therefore generation of new wetting fronts are infrequent. Accordingly, we see very similar soil moisture profiles for the top two soil layers throughout the Fort Assiniboine simulation between the LGAR model and HYDRUS-1D, but the deeper soils tend to be wetter in the HYDRUS-1D Fort Assiniboine simulation. Because precipitation partitioning is largely controlled by the soil hydraulics and soil moisture of the upper layers, the wetter, deeper soils in the HYDRUS-1D simulation do not impact the precipitation partitioning dynamics as significantly. It is also noteworthy that the characteristics of the forcing data and soil hydraulics will usually determine how deep the top most wetting front extends thus controlling the region of soil from which water is extracted to satisfy AET demand in LGAR. For example, frequent precipitation will more often ensure that the topmost wetting front is within the top layer, such that the region from which AET is extracted is fairly small, while infrequent precipitation allows more time for the most superficial wetting front to propagate among multiple layers. This theoretically impacts how well AET matches between LGAR and HYDRUS-1D. Again, determining the ideal AET regime for LGAR, or how this is impacted by various factors, we leave for future work.

5.3. Computational Advantage

While many RE solvers have been highly optimized for the large computational burden the RE presents, the LGAR concept has inherent computational advantages. Rather than requiring discretization of the vadose zone

into hundreds of nodes, LGAR creates state variables, (Z, θ) pairs, with new precipitation events and removes them when wetting fronts merge. The LGAR model therefore requires far fewer state variables per simulation. LGAR is also inherently mass conservative, where the RE faces an intrinsic relationship between error tolerance and runtime. We currently see that the LGAR model runs faster than corresponding simulations with the RE, and future work will focus on further computational optimization.

Perhaps more importantly, LGAR offers advantages in terms of reliability. Resolution of sharp wetting fronts by the RE, which can occur when using specific soil hydraulic parameters, discretization choices, and forcing data, potentially cause RE solvers to not converge. In contrast, particular combinations of these factors do not cause the LGAR model to fail. This is desirable, for example, when precipitation partitioning must be simulated over a spatially large model domain, over which it is not feasible to manually investigate and correct the causes of model nonconvergence.

6. Conclusions

The numerical solution of the Richards equation (RE) is the standard for simulating infiltration, soil moisture dynamics and precipitation partitioning, albeit with demanding discretization requirements that can affect accuracy, runtime and stability, particularly in the case of rainfall on initially dry, fine textured soils typical of arid and semi-arid regions. The original Green and Ampt (G&A) infiltration model provides a parsimonious two-parameter alternative for simulation of infiltration and precipitation partitioning. However, the original G&A model is limited to post-ponding simulations after a single intense rainstorm on deep, well-drained, homogeneous soils. Incremental advancements of the original G&A infiltration model have preserved part of the original concept—namely, soil moisture dynamics and precipitation partitioning can be explained with hydraulic conductivity and capillary suction. Further, all G&A—like methods simulate wetting fronts as discrete objects represented by the state variables Z (depth) and θ (volumetric water content). Because of the ubiquity of layered soils, the LGAR method described in this manuscript represents an advancement over Green and Ampt with Redistribution (GAR) methods. In multi-month simulations forced with measured rainfall, LGAR infiltration simulation results achieve KGE and NSE values that are close to 1 when compared against RE results in predicting infiltration and calculated runoff. Positive results were also observed in shorter simulations on the time scale of hours using idealized forcing data. The LGAR method requires the same inputs as both HYDRUS-1D and previously developed GAR methods. Because the LGAR method is not linked to groundwater its application is limited to arid or semi-arid climates, or at least in areas where the PET exceeds precipitation on average and the groundwater table is far from the land surface. Perhaps most importantly, the LGAR method is fast, reliable, and robust, while guaranteed to conserve mass. While having a difference from the RE that is well within the limits of uncertainty of soil hydraulic properties and parameters. In summary, LGAR is a computationally efficient method that accurately emulates RE results of infiltration into layered soils on a continuous basis, for arid or semi-arid climates.

Conflict of Interest

The authors declare no conflicts of interest relevant to this study.

Data Availability Statement

LGAR as implemented in Python, along with example simulation results, can be seen in the corresponding citation entry: La Follette and Ogden (2023). LGAR is currently being implemented in C as well. Videos showing LGAR example simulations can be found under the citation entry for La Follette (2022). USDA SCAN data (NRCS, 2023d) were adapted from sites whose general descriptions are viewable at NRCS (2023e) for Fort Assiniboine, NRCS (2023f) for Phillipsburg, and NRCS (2023g) for Bushland. For soil hydraulic parameters, data are viewable at NRCS (2023a) for Fort Assiniboine, NRCS (2023b) for Phillipsburg, and NRCS (2023c) for Bushland. Alternatively, these data are available via searching for their user pedon IDs of: 92MT041003, 04KS147001, and 91TX381001, respectively, on the URL cited in NRCS (2023d).

Acknowledgments
This work was funded by the National Oceanic and Atmospheric Administration (NOAA) under contract EA133W17BA0042/1305M220FNWWY0263. The LGAR model's development has been greatly aided by a number of people. Keith Jennings provided support for designing the structure of the LGAR code, discussions related to the formulation of actual evapotranspiration, suggestions for and feedback on how to visualize model results, assistance in interpretation of various options for lower boundary condition, and general support which helped to focus the direction of the project. Rachel McDaniel provided feedback on model results and logistically supported the project. Scott Peckham provided extensive support in implementing basic model interface (BMI) compatibility, suggested changes to the LGAR code as implemented in Python which increased its speed, and discussions about the formulation of the capillary drive term *G*. Jessica Garrett assisted in testing the LGAR model for basic model interface (BMI) compatibility.

References

Beven, K. (1982). On subsurface stormflow: An analysis of response times. *Hydrological Sciences Journal*, *27*(4), 505–521. https://doi.org/10.1080/02626668209491129

Beven, K. (1984). Infiltration into a class of vertically non-uniform soils. *Hydrological Sciences Journal*, *29*(4), 425–434. https://doi.org/10.1080/02626668409490960

Bocskor, Á., Hunyadi, M., & Vince, D. (2017). National Academies of Sciences, Engineering, and Medicine (2015) The Integration of Immigrants into American Society. Washington, DC: The National Academies Press. 458 pages. *Intersections: East European Journal of Society and Politics*, *3*(3), 157–161.

Chen, S., Mao, X., & Wang, C. (2019). A modified Green-Ampt model and parameter determination for water infiltration in fine-textured soil with coarse interlayer. *Water*, *11*(4), 787. https://doi.org/10.3390/w11040787

Chu, X., & Mariño, M. A. (2005). Determination of ponding condition and infiltration into layered soils under unsteady rainfall. *Journal of Hydrology*, *313*(3–4), 195–207. https://doi.org/10.1016/j.jhydrol.2005.03.002

Corradini, C., Melone, F., & Smith, R. E. (1994). Modeling infiltration during complex rainfall sequences. *Water Resources Research*, *30*(10), 2777–2784. https://doi.org/10.1029/94wr00951

Corradini, C., Melone, F., & Smith, R. E. (2000). Modeling local infiltration for a two-layered soil under complex rainfall patterns. *Journal of Hydrology*, *237*(1–2), 58–73. https://doi.org/10.1016/s0022-1694(00)00298-5

Corradini, C., Flammini, A., Morbidelli, R., & Govindaraju, R. (2011). A conceptual model for infiltration in two-layered soils with a more permeable upper layer: From local to field scale. *Journal of Hydrology*, *410*(1–2), 62–72. https://doi.org/10.1016/j.jhydrol.2011.09.005

Corradini, C., Morbidelli, R., Flammini, A., & Govindaraju, R. S. (2011). A parameterized model for local infiltration in two-layered soils with a more permeable upper layer. *Journal of Hydrology*, *396*(3–4), 221–232. https://doi.org/10.1016/j.jhydrol.2010.11.010

Cui, G., & Zhu, J. (2017). Infiltration model in sloping layered soils and guidelines for model parameter estimation. *Hydrological Sciences Journal*, *62*(13), 2222–2237. https://doi.org/10.1080/02626667.2017.1371848

Deng, P., & Zhu, J. (2016). Analysis of effective Green–Ampt hydraulic parameters for vertically layered soils. *Journal of Hydrology*, *538*, 705–712. https://doi.org/10.1016/j.jhydrol.2016.04.059

Downer, C. W., & Ogden, F. L. (2004). Appropriate vertical discretization of Richards' equation for two-dimensional watershed-scale modelling. *Hydrological Processes*, *18*(1), 1–22. https://doi.org/10.1002/hyp.1306

Farthing, M. W., & Ogden, F. L. (2017). Numerical solution of Richards' equation: A review of advances and challenges. *Soil Science Society of America Journal*, *81*(6), 1257–1269. https://doi.org/10.2136/sssaj2017.02.0058

Green, W. H., & Ampt, G. (1911). Studies on soil physics. *The Journal of Agricultural Science*, *4*(1), 1–24. https://doi.org/10.1017/s0021859600001441

La Follette, P. (2022). HydroShare video of LGAR [Dataset]. HydroShare. https://doi.org/10.4211/hs.46747d77d0ce4995b1e1d58384e15a09

La Follette, P., & Ogden, F. L. (2023). LGAR code in Python as of publication of related paper [Software]. HydroShare. https://doi.org/10.4211/hs.90951d952b034e7aa592898ab6d264eb

Lai, W., Ogden, F. L., Steinke, R. C., & Talbot, C. A. (2015). An efficient and guaranteed stable numerical method for continuous modeling of infiltration and redistribution with a shallow dynamic water table. *Water Resources Research*, *51*(3), 1514–1528. https://doi.org/10.1002/2014wr016487

Liu, J., Zhang, J., & Feng, J. (2008). Green–Ampt model for layered soils with nonuniform initial water content under unsteady infiltration. *Soil Science Society of America Journal*, *72*(4), 1041–1047. https://doi.org/10.2136/sssaj2007.0119

Ma, Y., Feng, S., Zhan, H., Liu, X., Su, D., Kang, S., & Song, X. (2011). Water infiltration in layered soils with air entrapment: Modified Green-Ampt model and experimental validation. *Journal of Hydrologic Engineering*, *16*(8), 628–638. https://doi.org/10.1061/(asce)he.1943-5584.0000360

Mohammadzadeh-Habili, J., & Heidarpour, M. (2015). Application of the Green–Ampt model for infiltration into layered soils. *Journal of Hydrology*, *527*, 824–832. https://doi.org/10.1016/j.jhydrol.2015.05.052

Morel-Seytoux, H., & Khanji, J. (1974). Derivation of an equation of infiltration. *Water Resources Research*, *10*(4), 795–800. https://doi.org/10.1029/wr010i004p00795

Mualem, Y. (1976). A new model for predicting the hydraulic conductivity of unsaturated porous media. *Water Resources Research*, *12*(3), 513–522. https://doi.org/10.1029/wr012i003p00513

NRCS. (2023a). Estimated soil water retention curve [Dataset]. United States Department of Agriculture. https://ncsslabdatamart.sc.egov.usda.gov/rptExecute.aspx?p=19462&r=6&

NRCS. (2023b). Estimated soil water retention curve [Dataset]. United States Department of Agriculture. https://ncsslabdatamart.sc.egov.usda.gov/rptExecute.aspx?p=31339&r=6&

NRCS. (2023c). Estimated soil water retention curve [Dataset]. United States Department of Agriculture. https://ncsslabdatamart.sc.egov.usda.gov/rptExecute.aspx?p=18826&r=6&

NRCS. (2023d). National cooperative soil survey soil characterization database [Dataset]. United States Department of Agriculture. http://ncsslabdatamart.sc.egov.usda.gov/

NRCS. (2023e). Pedon description [Dataset]. NASIS. https://ncsslabdatamart.sc.egov.usda.gov/rptExecute.aspx?p=19462&r=4&g=on&submit1=Get+Report

NRCS. (2023f). Pedon description [Dataset]. NASIS. https://ncsslabdatamart.sc.egov.usda.gov/rptExecute.aspx?p=31339&r=4&g=on&submit1=Get+Report

NRCS. (2023g). Pedon description [Dataset]. NASIS. https://ncsslabdatamart.sc.egov.usda.gov/rptExecute.aspx?p=18826&r=4&g=on&submit1=Get+Report

Ogden, F. L., Allen, M. B., Lai, W., Zhu, J., Seo, M., Douglas, C. C., & Talbot, C. A. (2017). The soil moisture velocity equation. *Journal of Advances in Modeling Earth Systems*, *9*(2), 1473–1487. https://doi.org/10.1002/2017ms000931

Ogden, F. L., & Saghafian, B. (1997). Green and Ampt infiltration with redistribution. *Journal of Irrigation and Drainage Engineering*, *123*(5), 386–393. https://doi.org/10.1061/(asce)0733-9437(1997)123:5(386)

Or, D. (2008). Scaling of capillary, gravity and viscous forces affecting flow morphology in unsaturated porous media. *Advances in Water Resources*, *31*(9), 1129–1136. https://doi.org/10.1016/j.advwatres.2007.10.004

Or, D., Lehmann, P., & Assouline, S. (2015). Natural length scales define the range of applicability of the Richards equation for capillary flows. *Water Resources Research*, *51*(9), 7130–7144. https://doi.org/10.1002/2015wr017034

Raats, P. A., & Knight, J. H. (2018). The contributions of Lewis Fry Richardson to drainage theory, soil physics, and the soil-plant-atmosphere continuum. *Frontiers in Environmental Science*, *6*, 13. https://doi.org/10.3389/fenvs.2018.00013

Richards, L. (1931). Capillary conduction of liquids through porous mediums. *Physics*, *1*(5), 318–333. https://doi.org/10.1063/1.1745010
Richardson, L. F. (1922). *Weather prediction by numerical process*. University Press.
Schaap, M. G., & Van Genuchten, M. T. (2006). A modified Mualem–van Genuchten formulation for improved description of the hydraulic conductivity near saturation. *Vadose Zone Journal*, *5*(1), 27–34. https://doi.org/10.2136/vzj2005.0005
Selker, J. S., Duan, J., & Parlange, J.-Y. (1999). Green and Ampt infiltration into soils of variable pore size with depth. *Water Resources Research*, *35*(5), 1685–1688. https://doi.org/10.1029/1999wr900008
Simunek, J., & Sejna, M. (2018). *HYDRUS pressure head reduction - S-shape*. PC Progress. Retrieved from http://www.pc-progress.com/en/OnlineHelp/HYDRUS3/Hydrus.html?PressureHeadReductionSShape.html
Simunek, J., Van Genuchten, M. T., & Sejna, M. (2005). *The HYDRUS-1D software package for simulating the one-dimensional movement of water, heat, and multiple solutes in variably-saturated media* (Vol. 3, pp. 1–240). University of California-Riverside Research Reports.
Sinai, G., & Dirksen, C. (2006). Experimental evidence of lateral flow in unsaturated homogeneous isotropic sloping soil due to rainfall. *Water Resources Research*, *42*(12). https://doi.org/10.1029/2005wr004617
Smith, R. E., Corradini, C., & Melone, F. (1993). Modeling infiltration for multistorm runoff events. *Water Resources Research*, *29*(1), 133–144. https://doi.org/10.1029/92wr02093
Smith, R. E., & Parlange, J.-Y. (1978). A parameter-efficient hydrologic infiltration model. *Water Resources Research*, *14*(3), 533–538. https://doi.org/10.1029/wr014i003p00533
Talbot, C. A., & Ogden, F. L. (2008). A method for computing infiltration and redistribution in a discretized moisture content domain. *Water Resources Research*, *44*(8). https://doi.org/10.1029/2008wr006815
Van Genuchten, M. T. (1980). A closed-form equation for predicting the hydraulic conductivity of unsaturated soils. *Soil Science Society of America Journal*, *44*(5), 892–898. https://doi.org/10.2136/sssaj1980.03615995004400050002x
Warrick, A., & Yeh, T.-C. J. (1990). One-dimensional, steady vertical flow in a layered soil profile. *Advances in Water Resources*, *13*(4), 207–210. https://doi.org/10.1016/0309-1708(90)90042-3
Wheater, H., & Evans, E. (2009). Land use, water management and future flood risk. *Land Use Policy*, *26*, S251–S264. https://doi.org/10.1016/j.landusepol.2009.08.019
Zha, Y., Yang, J., Zeng, J., Tso, C.-H. M., Zeng, W., & Shi, L. (2019). Review of numerical solution of Richardson–Richards equation for variably saturated flow in soils. *Wiley Interdisciplinary Reviews: Water*, *6*(5), e1364. https://doi.org/10.1002/wat2.1364